ADVANCED ELECTRONIC MATERIALS Open Access
www.advelectronicmat.de

InGaZnO-Based Thin-Film Thermistors on PEEK Fabric for Green Smart Textiles

Albert Heinrich Lanthaler, Sahira Vasquez, Riccardo Zamboni, Michael Haller, Luisa Petti, Niko Münzenrieder, and Giuseppe Cantarella*

Electronic textiles (e-textiles) have recently achieved outstanding results, allowing fast and reliable systems to be directly integrated into fabrics and threads. However, based on the environmental impact of these systems, the improvement of their limited End-of-Life (EoL) strategies is nowadays a major challenge. For this reason, the development of a circular technology for the realization of e-textiles, aiming at waste reduction and support of materials recycling, is highly required. Herein, an innovative and fully recyclable integration of thin-film electronics on a biocompatible polyether ether ketone (PEEK) fabric is presented. Specifically, three different configuration of InGaZnO-based thin-film thermistors are investigated, comparing their capabilities and sustainability. The devices are characterized over a temperature range from 25 to 60 °C; besides their thermal response, reliable functionality under bending stress and for NO_2 gas detection are proven. To demonstrate a circular and yet green approach, the devices are dissolved in water and the textile substrate is reused for a 2^{nd} generation of thin-film sensors, achieving comparable performances with respect to the 1^{st} generation ones. This work represents a first comprehensive analysis of thin-film thermistors integrated with textiles for the realization of breathable, flexible, and recyclable e-textiles, with applications for daily routine, ranging from automotive to human health monitoring.

1. Introduction

The textile industry has long played a pivotal role in human society, providing essential functions such as protection, temperature control, and disease prevention. In recent years, the industry has also become a key player in sustainability and innovation, driven by increasing societal demands for functional, robust, and environmentally friendly products.[1] Modern textiles have evolved to incorporate advanced features such as antimicrobial properties, water repellency, and protection from UV radiations and chemicals, broadening their applications across various fields.[2,3] Despite these advancements, the textile industry faces significant environmental challenges. Annually, over 92 million tons of textile waste are generated worldwide, with less than 20% being recycled or reused. Although 95% of textiles are technically recyclable, a substantial portion still ends up in landfills or is incinerated, increasing pollution and resource wastage.[4,5] Therefore, it is pivotal to develop strategies to increase the sustainability of the textile sector, through different approaches, including recyclability and waste valorization.

In parallel to this, the integration of electronics into textiles, fabrics, and yarns, creating so-called electronic textiles (e-textiles), offers promising solutions to enhance the functionality in areas such as healthcare, sportswear, entertainment applications, electricity generation, military, aerospace, and automotive industries.[6–11] This has allowed the integration of different electronics devices, such as transistors,[12–15] lighting and display,[16,17] photovoltaic cell,[18,19] alongside with sensors, such as biological,[20] sweat,[21–23] and temperature[24–26] detectors for on-skin applications. Among different alternatives, watersoluble[27] Indium-Gallium-Zinc-Oxide (IGZO) has been widely investigated as sensitive element for sensors, proving distinguishable sensitivities to pressure,[28] pH,[29] NO_2 gas,[30] humidity,[31] temperature,[32] and strain.[33]

Although different approaches for the integration of textiles and electronics have been proposed,[6–26] significant barriers exist for the wide adoption of e-textiles, including poor material performance and sustainability, complicated and

A. H. Lanthaler, S. Vasquez, R. Zamboni, M. Haller, L. Petti, N. Münzenrieder
Faculty of Engineering
Free University of Bozen-Bolzano
Bozen-Bolzano 39100, Italy
E-mail: albertheinrich.lanthaler@student.unibz.it

G. Cantarella
Department of Physics
Informatics and Mathematics
University of Modena and Reggio Emilia
Modena 41125, Italy

G. Cantarella
Istituto Nanoscienze CNR
Centro S3, via G. Campi 213/A, Modena 41125, Italy

The ORCID identification number(s) for the author(s) of this article can be found under https://doi.org/10.1002/aelm.202500146

DOI: 10.1002/aelm.202500146

time-consuming fabrication methods, and numerous toxic wastes generated from manufacturing processes.[34] Furthermore, e-textiles limited traceability complicates their EoL processing: despite several electronic components and materials employed in the device stack are valuable and not harmful, some others are based on hazardous heavy metals or halogenated organic compounds that can harm human health and pose environmental risks.[35] As a matter of fact, a transition from toxic (e.g., Cadmium (Cd),[36] Aluminum (Al),[37] and Copper (Cu)[38]) to low toxic metals (e.g., Silver (Ag),[39] Zinc (Zn),[40] and Magnesium (Mg)[41]) is an unmeant need for the fabrication of electrodes and circuits. Moreover, sustainable manufacturing processes and an effective EoL strategy are needed to address environmental concerns. This would lead to new smart and sustainable e-textiles which could either be recycled to value-added products or decomposed without any negative environmental impacts.[42] To create more sustainable e-textiles the first step is the employment of a green supporting carrier, represented by a yarn, a thread or a fabric. Some example can be found in natural fiber-based textiles, such as cotton,[43,44] hemp,[45,46] bamboo[47] and wool,[48] alongside with bio-compatible plastics based fibers (e.g., Polycarbonate (PC),[49] Polymethyl Methacrylate (PMMA)[50] and polylactic acid (PLA).[51] Polyether ether ketone (PEEK) is a biocompatible, semicrystalline, chemically inert and hydrophobic thermoplastic.[52] PEEK's hydrolysis resistance and excellent thermal and mechanical properties have attracted significant interest in aerospace and automotive industries.[53,54] Nowadays, PEEK-based textiles can be coated with metals like Ag via wet chemical processes,[55] Cu by DC sputtering,[56] and titanium (Ti) by e-beam evaporation[57] for applications including strain sensing and human body temperature monitoring. Next, substrate preparation and surface smoothing protocols, such as textile pre-treatments or planarization layers, need to have minimum carbon footprint. For the planarization layer, dip-coating and soaking techniques are viable solutions, due to their cost-effectiveness and applicability across various substrates, including metals, ceramics, polymer films, and fibrous materials too.[58–62] Common coating materials for smart textiles include polystyrene (PS),[63] Polypropylen (PP),[64] PLA,[64] and Polyuretane (PU).[65] Polyvinyl alcohol (PVA) stands out due to its biodegradability, biocompatibility, chemical stability, and easy processing.[66] PVA's safety is well-established, with low oral toxicity and no accumulation in the body.[67] Furthermore, this compound has been widely investigated as coating layer for smart textile fabrication, aiming at improve the deposition of thin-film materials (Cu, Ti, and stainless steel),[68]), AgNPs[69] and nano graphitic carbon nitride[70] on woven cotton fabric. Although green substrates and planarization layers have been reported, no results ever demonstrated the realization of recyclable thin-film device on an environmentally friendly textile system. Besides the employment of this innovative textile substrate, the key innovation on the recyclability side is twofold: first, the demonstration of a natural and yet green EoL strategy for the devices in water; second, the recovery of the substrate for an additional fabrication run, aiming at zero waste creation. **Figure 1** depicts the reliable integration of a recyclable PEEK-based fabric and dissolvable thin-film thermistors, proving the realization of a circular and yet sustainable smart textile. Using IGZO as the sensing element, three metals with different toxicity, such as Zn, Al, and Ag, were evaluated as electrodes. Devices were tested over a temperature range from 25 to 60 °C and their functionality was proved under mechanical bending stress. Lastly, sensor dissolution, as EoL strategy, and textile reuse were demonstrated for the implementation of a working second generation electronic device. This work represent a leap forward in the implementation of on-skin smart textiles with reduced carbon footprint and yet bespoke properties, including thermal response, mechanical flexibility, gas sensing, breathability and sustainability.

2. Results and Discussion

As depicted in the **Figure 1** inset, the proposed IGZO-based thermistors were directly fabricated on 80 µm-thick PEEK fabric coated with a thin PVA planarization layer. The PVA coating process had to take into account many different parameters, to satisfy specific needs related to the final application. In this regards, factors such as conformability, flexibility, and breathability have to be considered once aiming at systems in contact with human-body.[71] Specifically, breathability has a direct implication with the planarization layer applied on the carrier substrate.[72] Thus, after the cleaning process, a comparative study soaking the proposed fabric into a PVA water-based solution for different times (i.e., 0 s, 1, 3, 5, 10, and 30 min - **Figures S1** and **S2**, Supporting Information) was performed (Experimental Section - PVA soaking study). The 1 min soaking time was chosen as the most suitable. It utilizes the less PVA (RAR = 2.3 ± 0.5 mgm^{-1} m^2), it has a moderate stiffness (BS = 10.7 ± 6.0 mgcm) and it maintains breathability (WVTR = 0.978 ± 0.203 $kg\,m^{-2}\,h^{-1}$).

To evaluate the capability of this technology, thin-film devices were realized and electrically characterized on top of the planarized PEEK textile. **Figure 2a,b** depict the proposed substrate for electronic fabrication, based on a mesh of 241 by 217 µm holes of a commercial PEEK fabric coated with 5.30 µm-thick (1 min) PVA planarization layer (**Figure S2a**, Supporting Information); zooming in (**Figure 2b**), thanks to the PVA coating, an improved surface smoothness is achieved compared to non-coated textile, ready for the electronic fabrication. A picture of the proposed thin-film thermistors is presented in **Figure 2c**. For the layer structuring and deposition, the intrinsic properties of the PEEK substrate were considered. In particular, flake delamination occurring at temperatures above 70 °C,[56] has driven the choice toward room temperature depositions, to prevent substrate heating and consequent damages. For this reason, room temperature sputtering was selected for metals (Al, Zn, and Ag) and semiconductor (IGZO) depositions, in combination with vinyl tape-based shadow masking, as layer structuring method. The latter allowed better adhesion between the mask and the substrate, avoiding any electrodes short circuits caused by shadow effects. In addition, it minimized potential deterioration on PVA with respect to other techniques (e.g., photolithography) and during wet processing steps. Photolithography represents a possible further study for device patterning, specifically considering its low resolution (below 5 µm). However, considering the employment of different chemicals, the focus was devoted to a more sustainable fabrication process. Although our study implies device resolution (≈1 mm), the fabrication speed and large-area scalability are chosen as key parameters. More details can be found in **Table S3** (Supporting Information).

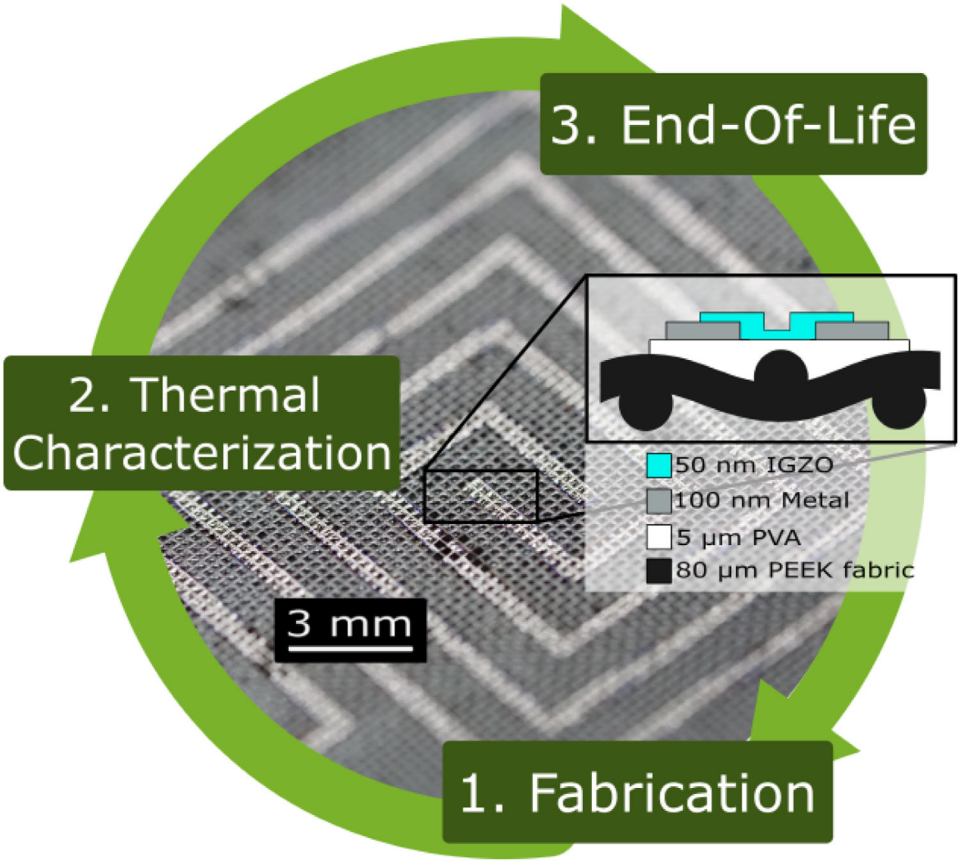

Figure 1. Recyclable integration of a breathable and dissolvable thin-film thermistor onto a biocompatible fabric. Inset: schematic presentation of the proposed devices, based on 80 µm-thick PEEK fabric, 5 µm-thick PVA planarization layer, 100 nm Metal contacts, 50 nm IGZO layer.

Through the combination of thin-film materials, three different thermistors were realized and their performance compared: Al-IGZO, Zn-IGZO, and Ag-IGZO. After electronic fabrication, the presented devices showed an average resistance of $2 \times 10^4\ \Omega$, $50 \times 10^2\ \Omega$, $1 \times 10^6\ \Omega$ for the Al-, Zn-, and Ag-based, respectively. The devices' output between $1 \times 10^2\ \Omega$ and $1 \times 10^6\ \Omega$ proves either the formation of ohmic contact between the metal electrodes and the IGZO sensitive layer, and a good adhesion of the electronic on the PEEK-PVA textile based substrate. The combination of the chosen PVA coating layer, thinner compared to textiles with longer soaking time, and the sputtering fabrication process have led to a change of the final device breathability. **Figure** 3a,b reports both the macroscopic and microscopic view of a final device, showing an average hole density of $12\ mm^{-2}$ on the planaritazion layer, 77.7% of the fresh PEEK fabric's value, which brought to a comparable WVTR (**Table** S4,

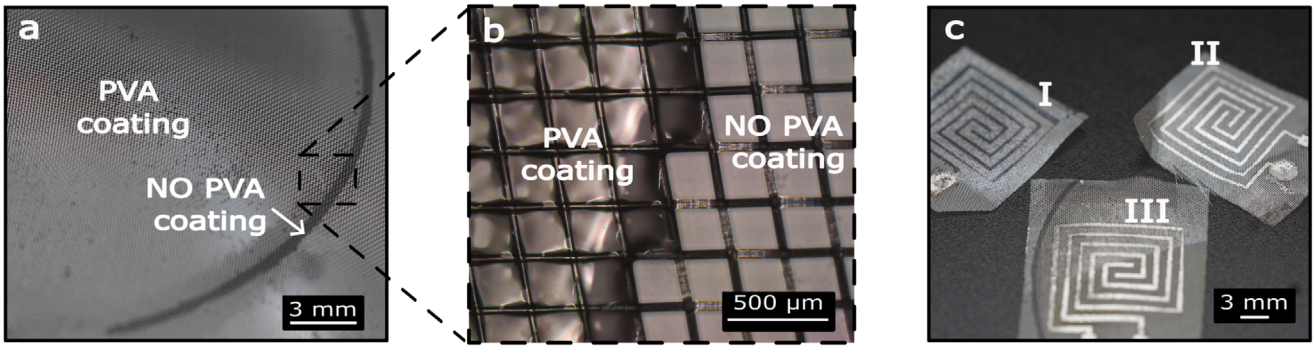

Figure 2. Thin-Film Thermistors' integration on PEEK fabric. a) Picture and b) zoom-in view of the proposed PEEK-PVA coated fabric (5.30 µm-thick coating layer), reporting two areas: a PVA fully coverage of the fabric matrix, and the PEEK fabric not coated. c) Picture of the proposed IGZO-based thermistors after device fabrication: I) Zn-based, II) Al-based and III) Ag-based devices.

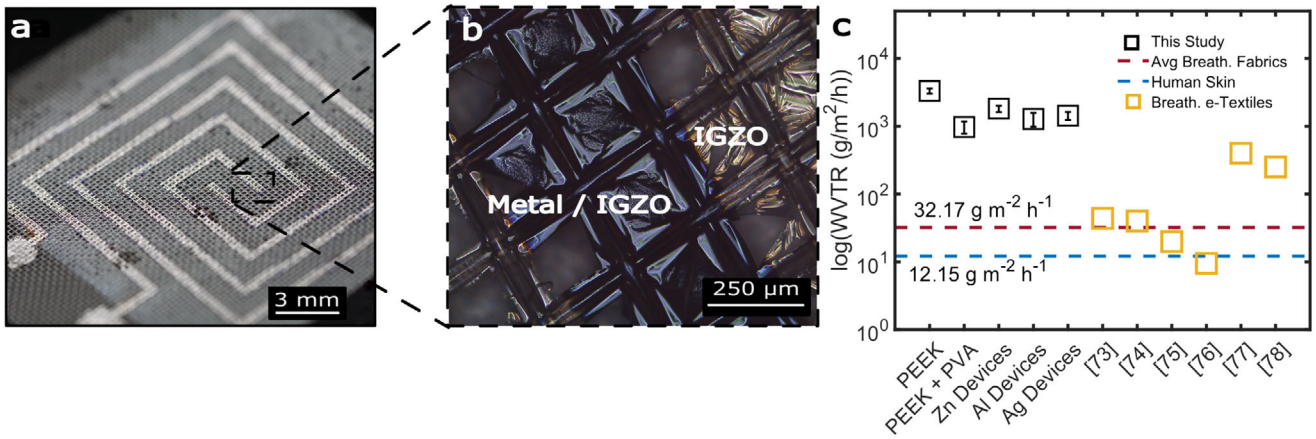

Figure 3. Effect of planarization layer coating. a) Optical image and b) zoom-in view of the proposed Thermistors on a PEEK-PVA coated fabric: two different regions, coated with Metal-IGZO and IGZO only, are visible. c) WVTR values for the textile at different fabrication steps: fresh (PEEK), after coating with PVA planarization layer (PEEK+PVA) and after Thermistors fabrication (Zn, Al, Ag devices); values from this study are shown as black square. Breathable Smart Textiles WVTRs are reported as yellow square.[73–78] Average value of Breathable fabrics WVTRs[79] is reported as magenta dot-line. The average Human Skin[80,81] is also reported as reference (blue dotted line). All values are plotted on a log scale for clarity.

Supporting Information). The high vacuum conditions during the thin-film depositions have raised the three final devices breathability (**Figure** 3b). For the complete electronics stack, the breathability resulted in a WVTR of and average 1281 g/ m^2 h^{-1} within the three of them, 65% more breathable than the PEEK-PVA coated value. Commercially available breathable fabrics[79] (magenta dashed-line, **Figure** 3c) and average Human Skin[80,81] WVTRs (blue dashed-line, **Figure** 3c) are reported as reference. Thanks to PEEK-fabric holes area (≈52300 µm^2) the presented devices are three times better compared with others breathable smart textiles, such as Motion Detector,[73] Pressure Sensor,[74] Multifunctional Textile,[75] Epidermal Device,[76] Multi-modal smart wearable,[77] and Human Health Management system,[78] (yellow squares, **Figure** 3c and **Table** 1). Once the breathability has been proven even after electronic fabrication, temperature sensitivity was tested for the proposed devices. The thermal characterization of the thermistors was evaluated in a sealed gas chamber, varying the temperature from 25 to 60 °C in steps of 5 °C, while keeping the relative humidity constant at 26 ± 3% (Experimental Section - Thermal and Gas Characterizations).

The hysteresis of the three different thermistors was evaluated by repeating the heating and cooling cycle for three times. As expected for these devices, the as-fabricated thermistors show decrease (increase) of the normalized electric resistance once raising (lowering) the temperature. In particular, after a stabilization time of 100 min, reliable functionality is reported for Al-based thermistors (**Figure** 4a). From the very last heating-cooling cycle, the calibration curve (Figure 4b) was calculated, extracting, after an assessment time of 10 s each step, mean and standard deviation of the resistance value of both heating and cooling cycle at the same temperature step. A sensitivity (Temperature Coefficient of Resistance, TCR) of -8.4×10^{-3} °C^{-1} (R^2 = 0.99) was reported, showing linear behavior, 2.27% maximum hysteresis and 1% deviation from the zero condition at 25 °C.

Zn-based thermistors (**Figure** 4c) showed a different behavior: after a proper output resistance during the first heating and cooling cycle, a loss of contact (grey area) was experienced and sensors were not anymore conductive. At the same time, even if the reading output showed 2.32% maximum hysteresis, reaching almost the same value between heating and cooling stages, zero condition return was strongly affected by an unexpected resistance drop. **Figure** 4d reports a sensitivity of -7×10^{-4} °C^{-1} (R^2 = 0.76). Lastly, Ag-based thermistors (**Figure** 4e) reported a 3.34% maximum hysteresis and a variation of 1% on the zero returning condition. Moreover, Ag-based thermistors reported a behavior comparable with Al-based (**Figure** 4f), showing a sensitivity of -1.5×10^{-2} °C^{-1} (R^2 = 0.99). A summary of the temperature characteristics is reported in **Table** S5 (Supporting Information).

Textiles, fabrics and threads are capable of resisting stress (e.g., mechanical bending, stretching, folding, and abrasion) for enormous amount of repetition during their entire life cycle. Although the PVA planarization layer increased the bending stiffness of the fabric, its flexibility was not much affected. For this reason, the device performance variation under mechanical bending stress was object of study beside the electrical characterization. **Figure** 5a reports a representative thermistor 3D image during the mechanical characterization while bent down to 3 mm bending radius over 1000 times. The maximum compressive strain applied to the temperature sensor was calculated as 1.08% (**Equation** 5). The output static resistance for each

Table 1. Water Vapour Transmission Rates (WVTRs) of six different smart textiles reported in literature.

Textile	Device	WVTR [g/ m^2 h^{-1}]	Refs.
Cotton	Motion Detector	43.76	[73]
Hemp	Pressure Sensor	40	[74]
Cotton	Multifunctional	19.92	[75]
PEEK	Thermistors	1281	This Work
TPU nanotextile	Epidermal Device	9.5	[76]
Sericinin-Graphite	Multi-modal	400	[77]
SEBS textile	Human Health Management	251.41	[78]

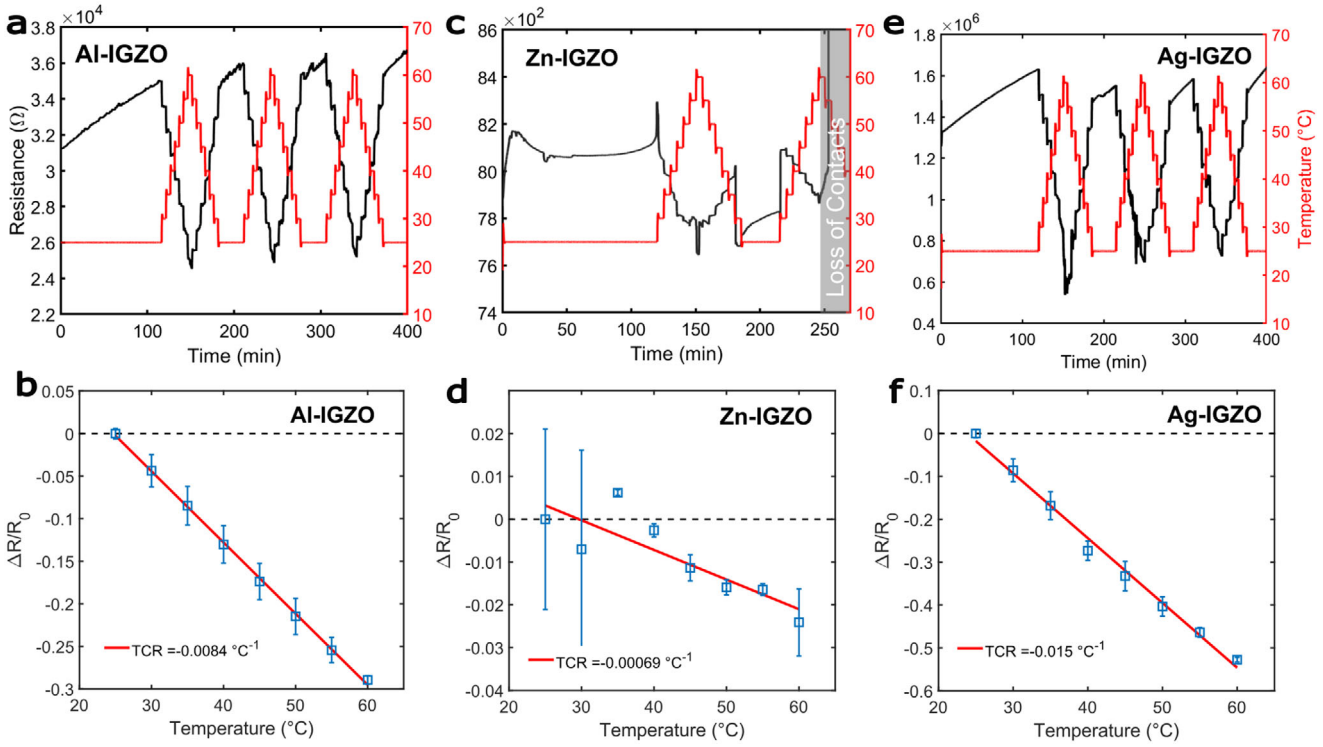

Figure 4. Temperature characterization of Al-IGZO, Zn-IGZO and Ag-IGZO thermistors. Resistance changing during cycling temperature variation, from 25 to 60 °C, repeated three time for a) Al-IGZO thermistors, c) Zn-IGZO thermisors and e) Ag-IGZO thermisors. Sensitivity, error and hysteresis from 25 °C to 60 °C, for b) Al-IGZO thermistors ($R^2 = 0.99$), d) Zn-IGZO thermisors ($R^2 = 0.76$) and f) Ag-IGZO thermisors ($R^2 = 0.99$).

device is reported, in flat (yellow) and bent (blue) conditions (see **Figure** 5b,c,d). The Al-based thermistors reported an increase in the output resistance, either in flat and bent conditions, with a 160% peak while bent down. The devices were not anymore conductive after 300 cycles. Zn-based sensors showed an output resistance increase in both flat and bent conditions as well, with a 200% peak while bent down. The devices were not anymore conductive after 266 cycles. Finally, Ag-based devices proved robustness and durability even after 1000 cycles. Here, an increase of the resistance was experienced, with a maximum increment of 7% while bent down. No significant differences were reported between the three devices: specifically, no cracks or damages were visible. Optical imaging was performed before and after bending test to evaluate the formation of flakes delamination, cracks or damages to the substrate and at the substrate-electronics interfaces, but none of them were reported. The leakage in cracks formation proves once again the presence of an optimal adhesion between either electrodes and IGZO layers, and between the thin-film electronics and the PEEK-PVA textile substrate. The underlying reason for such different behavior can be found in the fabrication process itself and specifically in the formation of native oxides: indeed, the shadow masking approach consists in two masks applied to the substrate, one for the metal contacts and, afterwards, one for the semiconductor layer. To allow the mask change, the samples have to be exposed to controlled environmental condition, the same for all the proposed devices: this exposure, even if for few minutes, facilitate the development of Zn[82] and Al[83] native oxides. Their thickness is depended to time exposure to air, varying from the formation of some nano-clusters up to ≈ 2 nm to 5 nm thick layers; moreover, inherent characteristics of Al_2O_3 and ZnO is their brittle failure deformation.[84,85] This brittle rupture wasn't reported for the Ag-based devices, proving the Ag-native oxide is negligible and it doesn't influence the overall performance of the system under mechanical bending. While the thermistors demonstrate stable functionality under the tested bending condition, a more comprehensive analysis under different deformation conditions is planned for future work to support wearable integration.

Afterwards, to prove that the mechanical strain has caused no damages on the thin-film device, a 2^{nd} thermal characterization of the Ag-based thermistor was carried out (Figure 5e), showing its capability to respond to thermal excitation even after a dynamic bending stress. Here, comparing the average sensitivity *Before* (-1.5×10^{-2} °C^{-1}) and *After* (-3.0×10^{-3} °C^{-1}), a variation of 80% was reported, due to the prolongate mechanical stress on the device after a 1000 cycle bending solicitation. Even if this study represents a first trial to fabricate thin film thermistors directly on a recyclable PEEK/PVA based fabric, the resistance output variation (ΔR) after 1000 cyclic mechanical bending (3 mm) of the Ag-based device is comparable with ΔR values reported in literature for thermistors fabricated on flexible plastic based substrates.[86–88]

Environmental condition monitoring and in particular gas detection sensing capability represent a promising frontier for e-textiles, allowing to widely open innovative safety applications for these smart systems. In this regards, taking advantage of the wide employment of IGZO as sensing element,[28–33] the presented devices have shown response to nitrogen compounds,

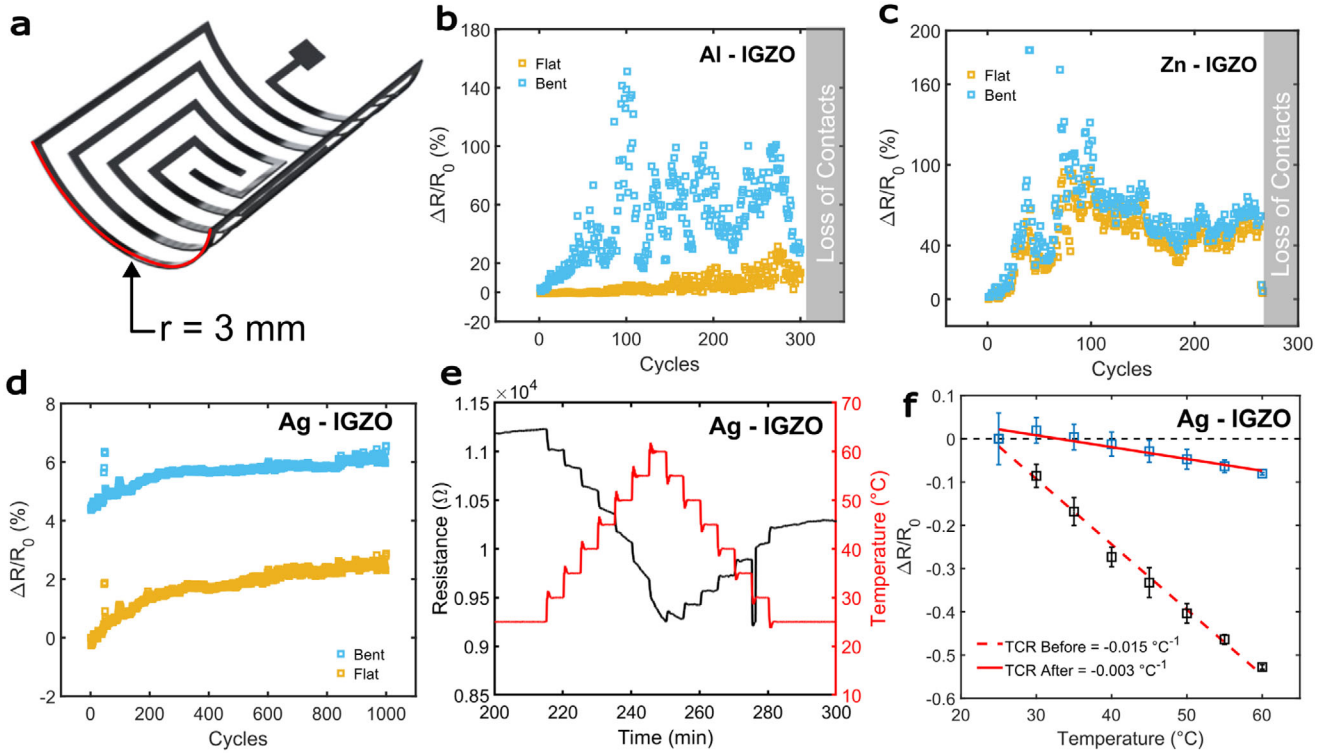

Figure 5. Mechanical characterization of Al-IGZO, Zn-IGZO, and Ag-IGZO thermistors. a) Thermistor bent down to 3 mm bending radius. Static resistance measurements during 1000 bending cycles at room temperature, either in bent and flat condition, of the proposed temperature sensors: b) Al-IGZO thermistors, c) Zn-IGZO thermisors and d) Ag-IGZO thermisors. e) Ag-IGZO thermistor perfomance evaluation after mechanical characterization (1000 bending cycles). f) Comparison between before and after ($R^2 = 0.91$) mechanical characterization of sensitivity, error and hysteresis of the proposed Ag-IGZO thermistors.

specifically NO_2. This gas can cause human body's infection and some respiratory diseases, such as bronchitis, pulmonary edema, and asthma: the Health and Safety Rule Alarm considered NO_2 one of the most dangerous gases, since the human body cannot stay more than 8 h in an environment with more than 3 ppm NO_2.[89,90] This makes NO_2 an important biomarker in human breath analysis for medical diagnostics.[91,92] Therefore, the response of the proposed devices to different NO_2 gas concentration was investigated in a custom gas chamber. **Table 2** reports the IGZO-based thermistors' responses to different NO_2 concentrations: the presented values are the average resistance response (%) of the proposed devices at the specific NO_2 gas concentration step (5 min each). The Al-based devices is not reported here, based on an inconsistent response at each step of the NO_2 gas concentration (**Figure** S6a, Supporting Information). On the other hand, the Zn-based devices demonstrated to be stable, having a variation of 64.73% at 50 ppm, although the devices' response was significantly interested by a high standard deviation at each step, as reported in **Figure** S6b (Supporting Information). Lastly, the Ag-based devices' response was strongly affected by a baseline drift (**Figure** S6c, Supporting Information), producing a mean 100% increase of the resistance value at each NO_2 gas step. The current results showcase that the device presented in this work could be a potential option for a wearable sensor to detect NO_2, but surely deeper analysis and further investigation are required beyond the scope of the current study.

Table 2. Sensors' responses to different NO_2 concentrations: the table summarizes the average response of Zn-IGZO and Ag-IGZO thermistors to different NO_2 concentrations. The Al-IGZO has been omitted due to its unclear or inconsistent response to the gas concentrations.

NO_2 concentrations	Zn-IGZO [%]	Ag-IGZO [%]
1 ppm	5.33	96.25
5 ppm	10.15	149.38
10 ppm	21.92	240.81
30 ppm	39.20	368.96
50 ppm	64.73	467.64

To accomplish a fully sustainable textile technology, it is pivotal to assess any EoL strategies for both the carrier and the electronics. One approach is to dissolve the thin-film electronics and the planarization layer, reusing the textile for a new generation of electronic devices. Since Ag-based thermistors showed the best electrical, thermal and mechanical behaviors, they were chosen for the dissolution and regeneration experiments afterwards. A water-based dissolution EoL process was chosen, taking advantage from the water-solubility of both the PVA and the IGZO layers. Although this method would last longer than others presented in literature,[93,94] it showed a lower environmental

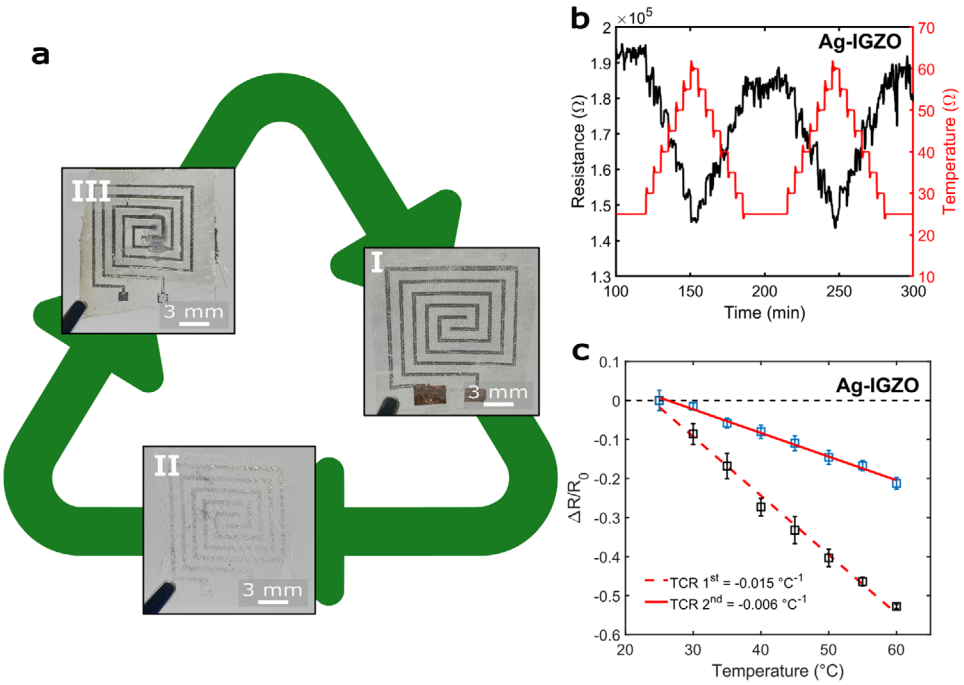

Figure 6. EoL Strategy and Reusability: a) Ag-IGZO thermisors second generation fabrication strategy, reporting: I) picture of the 1st Sensor Generation, II) picture of the 1st Sensor Generation after 18 days in DI Water at 60 °C and III) picture of the 2nd Sensor Generation after electronic fabrication. b) Resistance changing during cycling temperature variation, from 25 to 60 °C repeated three time of the Ag-IGZO 2nd sensor generation. c) Comparison between 1st and 2nd Ag-IGZO sensor generation of sensitivity, error and hysteresis from 25 °C to 60 °C ($R^2 = 0.99$).

impact (low energy consumption involved) and it avoided the use of harsh chemicals (see **Figure** S7, Supporting Information). The three-phase devices dissolution process is reported, starting from the 1st sensor generation (**Figure** 6a-I). After 18 days soaked in deionized (DI) water stirred at 60 °C, material residuals were still visible (**Figure** 6a-II), but no conduction was achievable, proving their dissolution. At this stage, once the substrate itself was cleaned from Ag leftovers, a second fabrication flow was performed, including a new PVA coating (5.30 µm-thick), acting as planarization layer, and the realization of a 2nd generation Ag-IGZO thermistors (**Figure** 6a-III). Once the devices proved to be conductive, the 2nd sensor generation was tested under same temperature condition as the

1st one (25 to 60 °C), showing reliable functionality at each temperature variation (**Figure** 6b). **Figure** 6c reports a comparison within the two generation calibration curves: the 2nd sensor generation showed a decay (60%) of the average temperature coefficient resistance, with a sensitivity of -6×10^{-3} °C^{-1} ($R^2 = 0.99$), proving the capability of being fully recyclable. Al-based and Zn-based thermistors' water solubility are reported in **Figure** S8 (Supporting Information). The 2nd sensor generation sensitivity was affected by a decay after its fabrication, potentially related to mechanical stress on the PEEK fabric matrix during devices dissolution. Based on this, further investigation will be carried out to better understand the full dissolution of the proposed devices and optimize their EoL processes throughout surface analysis and threads' material integrity study, to either improve recyclability and guarantee comparative sensitivity, focusing on the functional lifespan of the regenerated thermistors compared to the 1st Generation device.

3. Conclusion

In summary an innovative fabrication process for thermal sensitive, breathable and reusable IGZO-based thin-film thermistors on biocompatible PEEK fabric was achieved. Based on PEEK chemical, mechanical and thermal properties, fast PVA dip coating was possible, without reporting any swelling or distortion in the fabric matrix. Moreover, PEEK-PVA based substrate withstanded both DC and RF sputtering processes of conductive thin-film layers on top of it in vacuum condition. Devices' characterization consisted of three different analyses: first, a WVTR study was conducted to compare the three (Zn, Al, Ag-based) different thermistors' final breathability before and after the sputtering process, resulting in a general increment, above 1281 g/ m^2 h^{-1} (three times more breathable than other smart textiles).[73–78] Afterwards, thermistors' response to thermal stress was evaluated with three cycles of heating and cooling (25 °C to 60 °C), resulting in a sensitivity of -8.3×10^{-3}, -7×10^{-4}, and -1.5×10^{-2} °C^{-1}, for Al, Zn, and Ag, respectively, comparable with literature.[95–102] Lastly, cyclic bending performance up to 1000 times was tested, with minimal performance drift (i.e., 7%) down to 3 mm bending radius for the Ag-based thermistors, comparable with literature.[86–88] Supported by reliable device functionality, Ag-based sensors degradation and textile reuse were demonstrated as EoL strategy for the implementation of a 2nd generation electronic devices. New Ag-based thermistors, fabricated on refurbished PEEK, were tested under the same temperature cycle, reporting for the first time the reusability of textile to host a new generation of electronic devices. Further studies will be devoted to improve different aspects: first, the integration of such

an intriguing platform onto lower carbon-footprint and inherent biodegradable fabrics, such as cotton, bamboo, hemp, lotus, and linen. Second, additional investigation will be carried out on temperature range for wearable and near-body sensing applications or expanding to lower ranges for outdoor environmental scenarios. Moreover, the mechanical stability and device robustness will be investigated to fully understand the reliability of this devices under multiple stress conditions, optimizing the layers structure to decrease the thermistor sensitivity decay after bending (80%) without affecting the whole system's lightweight, flexibility, and breathability. Lastly, further studies will be devoted to the investigation and the calibration of the NO_2 response of the proposed devices, aiming at fabricating a multi-sensing platform. This work presents an innovative method to implement recyclable and breathable smart textiles designed for short-term use and reusable patches, with a perspective toward highly flexible and environmentally-friendly electronic devices.

4. Experimental Section

PEEK Fabric Characteristics: A commercial fuel filtering fabric of Polyether ether ketone (PEEKTEX IEM 17-195/70, SEFAR AG, Switzerland) was chosen as substrate for electronic fabrication. The fabric weight resulted in 11×10^{-4} g/ cm^2 . The fabric presented a woven structure (1:1) where warp and weft direction showed four threads per millimeter each. The average thread thickness was 37 µm for both direction while the average distance between two threads was 270 µm for the warp and 251 µm for the weft direction.

PVA Soaking Study - Relative Absorption Rate: The PEEK fabric was cleaned in an acetone and an isopropanol ultrasonic bath for 5 min each. Then, it was soaked in a PVA (Sigma–Aldrich®, Molecular Weight 89.000 gmol^{-1} to 98.000 gmol^{-1}) water-based solution (4.7%). Afterwards, five different fresh PEEK fabric were soaked for five different soaking time (e.g., 1, 3, 5, 10, and 30 min). **Table** S9 (Supporting Information) reports the PVA mass absorbed (mean and standard deviation) divided by area (Relative Absorption Rate, RAR) for all the five different soaking times. A clear trend was visible, reported also in **Figure** S2 (Supporting Information) optical profilometer measurements: the longer the soaking time, the more PVA is absorbed. The 1 min shows the better RAR (e.g., 2.3 mgm^{-1} m^2), based on a PVA layer of ≈5 µm-thick; the 3, 5, and 10 min samples reported to have the same RAR (3.4 mgm^{-1} m^2), since an average PVA layer of ≈100 µm was visible for the three of them (**Figure** S2b,c,d, Supporting Information). Lastly a formation of a thicker layer (i.e., ≈ 220 µm - **Figure** S2e, Supporting Information) and the highest RAR of the study (e.g., 6.4 mgm^{-1} m^2) for the 30 min soaking time was reported.

PVA Soaking Study - Bending Stiffness: To test the resulting bending stiffness of the substrate (PEEK fabric coated with different PVA planarization layers), a Shirley Bending Stiffness Tester (SBST) was utilized (**Figure** S10, Supporting Information).[103] Five different samples from each different soaking time (1, 3, 5, 10, and 30 min) were chosen, weighed (W) and its area (A) was measured (see **Table** S11, Supporting Information). Same process was done on a chosen fresh PEEK fabric sample. Then, each sample was placed on the flat part of the SBST, at the outer edge, and the initial position (L_i) was measured; after pushing and slightly moving, each sample dropped and touched the inclined part of the SBST and the final position (L_f) was measured. For each sample, the resulting measured length ($L = L_f - L_i$) was calculated. Finally, the resulting Bending Stiffness of each sample was calculated as follow:[104,105]

$$G = \frac{W \cdot (L \cdot f_1)^3}{A} \tag{1}$$

where f_1 is a function of the draping angle ϑ (41.5 °) of the SBST, expressed as:

$$f_1 = \sqrt[3]{\frac{cos(\frac{\vartheta}{2})}{(8 \cdot tan(\vartheta)}} \tag{2}$$

The overall trend confirms an increases accordingly to the RAR, proving the PVA planarization layer makes the fabric stiffer and less bendable. The 5 min sample drop is most likely related to a non-uniform layer formed, as it can be also see in **Figure** S2c (Supporting Information)

PVA Soaking Study - Water Vapor Transmission Rate: WVTR measurements were performed before and after electronic fabrication, in order to study the breathability of either the substrate (PEEK fabric coated with different PVA planarization layers) and the final devices. Each sample was taped with polymide tape on top of a half-full DI water cup, leaving an average open area of 221.56 mm^2 ; afterwards, the resulting Device Under Test (DUT: cup, polymide tape, DI water and the sample) was weighted. Next, the DUT was stored inside a climate chamber, controlling temperature and humidity conditions (36 °C and 50% RH) for 24 h. Finally, the DUT was weighed a second time to evaluate the liquid evaporated through the sample, allowing the calculation of the WVTR index as follows:[79,106]

$$WVTR = \frac{W}{A \cdot t} \tag{3}$$

where W is the amount of evaporated DI water divided by the area (A) of each sample and the evaporation process time (t = 24 h). **Table** S12 (Supporting Information) reports the Water Vapor Transmission Rate (WVTR) conducted, comparing the five different soaking times with the fresh PEEK fabric. As it could be seen, the water transmission decrease increasing the PVA absorbed by the fabric, proving that a thicker PVA planarization layer had been formed, accordingly with stiffer final system (fabric plus planarization layer). The 1 min soaking sample (0.978 ± 0.203 kg/ m^2 h^{-1}) and the 3 min sample (1.039 ± 0.123 kg/ m^2 h^{-1}) had the better WVTR, proving to produce the littler change (29% and 31%, respectively) in the original WVTR of the fresh PEEK fabric.

Electronics Fabrication: After the 1 min sample was selected, on each sample, a 100 nm-thick layer of Aluminunm (Al), Zinc (Zn), or Silver (Ag) was deposited by DC sputtering at room temperature. Lastly, on top of each metal layer, 50 nm IGZO from a ceramic target was RF sputtered at room temperature.

Thermal and Gas Characterizations: The electrical over temperature and NO_2 gas response of the sensors were carried out in a sealed chamber. Each pad of each sensor was coated with conductive silver paste, Cu tape and contacted with custom made needle contacts, monitoring temperature and relative humidity using a calibrated PT100 sensor and a Honeywell HIH-4000-001 sensor, respectively. A dedicated data acquisition system, including a high-performance digital multimeter (Keithley Model 2000 with 6 1/2 digits), a source measure unit (Keithley Series 2600B), and a custom LabView program were employed. For the NO_2-characterization, five concentrations (1, 5, 10, 20, and 30 ppm) of gas were injected into the chamber using mass flow controllers (dry air acted as the carrier gas); all measurements were conducted at room temperature (25 °C). The sensor response was evaluated using the normalized response formula:

$$\frac{R_i - R_0}{R_0} = TCR \cdot T_i \tag{4}$$

where R_0 is the resistances at the start of the experiment and R_i the average resistance at each temperature T_i.

Mechanical Characterization: To evaluate the mechanical performance, a custom-made bending machine (BM) was employed for cycling experiments. The mechanical characterization was done by taping each type of thermistor with a double side tape to a plastic-based trail (2 cm x 5 cm), concentrating the maximum stress in the middle region of the fabricated sensor. To improve the contact, each pad of each sensor was coated with conductive silver paste, Cu tape and Cu wires.

Finally, each temperature sensor was connected to either the static and dynamic stage of the BM, clamping the two contact pads with commercial crocodile clamps wired to a digital source meter (Keithley Series 2600B, USA). During each bending cycle, the resistance was monitored and collected through a custom-made LabView program. The compressive strain applied to the temperature sensor was estimated as 1.08% with the following equation:[107]

$$\epsilon_{top} = \frac{t_{sub} + t_{ele}}{2\rho} \quad (5)$$

where, ϵ_{top} is the strain at the electronic surface, t_{sub} is the substrate thickness, t_{ele} is the electronic layer thickness and ρ is the radius of curvature (ρ = substrate's length (L) / bending radius (r = 3 mm)).

Supporting Information

Supporting Information is available from the Wiley Online Library or from the author.

Acknowledgements

This study was partially funded by the European Union - NextGenerationEU, in the framework of the iNEST - Interconnected Nord-Est Innovation Ecosystem (iNEST ECS00000043 – CUP I43C22000250006) and by the Autonomous Province of Bozen-Bolzano, South Tyrol's European Regional Developmental Fund (ERDF) Program under Projects EFRE/FESR 1011 - SmartCover and EFRE/FESR 1007 - iPlayground. The views and opinions expressed were solely those of the authors and did not necessarily reflect those of the European Union, nor can the European Union be held responsible for them. The authors would like to thank SEFAR AG for providing the PEEK fabric.

Conflict of Interest

The authors declare no conflict of interest.

Data Availability Statement

The data that support the findings of this study are available from the corresponding author upon reasonable request.

Keywords

circular smart textile, sustainability, thin-film electronics

Received: April 25, 2025
Revised: June 27, 2025
Published online:

[1] N.-K. Persson, J. G. Martinez, Y. Zhong, A. Maziz, E. W. Jager, *Adv. Mater. Technol.* **2018**, *3*, 1700397.
[2] M. T. Hossain, M. A. Shahid, M. G. M. Limon, I. Hossain, N. Mahmud, *J. Open Innov.: Technol., Market, Complex.* **2024**, *10*, 100230.
[3] T. Tat, G. Chen, X. Zhao, Y. Zhou, J. Xu, J. Chen, *ACS Nano* **2022**, *16*, 13301.
[4] G. Lawton, *New Sci.* **2022**, *254*, 38.
[5] S. Weber, J. Lynes, S. B. Young, *Int. J. Consum. Stud.* **2017**, *41*, 207.
[6] H. L. O. Júnior, R. M. Neves, F. M. Monticeli, L. Dall Agnol, *Textiles* **2022**, *2*, 582.
[7] M. A. Shah, B. M. Pirzada, G. Price, A. L. Shibiru, A. Qurashi, *J. Adv. Res.* **2022**, *38*, 55.
[8] A. Giglio, K. Neuwerk, M. Haupt, G. M. Conti, I. Paoletti, *Textiles* **2022**, *2*, 296.
[9] K. Gasparini, *Textiles* **2022**, *2*, 436.
[10] G. N. Islam, A. Ali, S. Collie, *Cellulose* **2020**, *27*, 6103.
[11] M. Catrysse, R. Puers, C. Hertleer, L. Van Langenhove, H. Van Egmond, D. Matthys, *Sens. Actuators, A* **2004**, *114*, 302.
[12] A. Bonfiglio, D. De Rossi, T. Kirstein, I. R. Locher, F. Mameli, R. Paradiso, G. Vozzi, *IEEE Trans. Inf. Technol. Biomed.* **2005**, *9*, 319.
[13] N. Münzenrieder, C. Vogt, L. Petti, G. A. Salvatore, G. Cantarella, L. Büthe, G. Tröster, *Technologies* **2017**, *5*, 2.
[14] K. H. Cherenack, T. Kinkeldei, C. Zysset, G. Tröster, *IEEE Electron Device Lett.* **2010**, *31*, 740.
[15] S. J. Kim, H. Kim, J. Ahn, D. K. Hwang, H. Ju, M.-C. Park, H. Yang, S. H. Kim, H. W. Jang, J. A. Lim, *Adv. Mater.* **2019**, *31*, 1900564.
[16] X. Shi, Y. Zuo, P. Zhai, J. Shen, Y. Yang, Z. Gao, M. Liao, J. Wu, J. Wang, X. Xu, Q. Tong, B. Zhang, B. Wang, X. Sun, L. Zhang, Q. Pei, D. Jin, P. Chen, H. Peng, *Nature* **2021**, *591*, 240.
[17] H. W. Choi, D.-W. Shin, J. Yang, S. Lee, C. Figueiredo, S. Sinopoli, K. Ullrich, P. Jovančić, A. Marrani, R. Momentè, J. Gomes, R. Branquinho, U. Emanuele, H. Lee, S. Y. Bang, S.-M. Jung, S. D. Han, S. Zhan, W. Harden-Chaters, Y.-H. Suh, X.-B. Fan, T. H. Lee, M. Chowdhury, Y. Choi, S. Nicotera, A. Torchia, F. M. Moncunill, V. G. Candel, Durães, K. Chang, et al., *Nat. Commun.* **2022**, *13*, 814.
[18] J. Plentz, G. Andrä, T. Pliewischkies, U. Brückner, B. Eisenhawer, F. Falk, *Mater. Sci. Eng., B* **2016**, *204*, 34.
[19] B. O'Connor, K. P. Pipe, M. Shtein, *Appl. Phys. Lett.* **2008**, *92*, 172.
[20] S. Sonkusale, in *2022 IEEE Custom Integrated Circuits Conference (CICC)*. IEEE, Piscataway, NJ **2022**, pp. 01–07.
[21] J.-H. Ha, Y. Jeong, J. Ahn, S. Hwang, S. Jeon, D. Kim, J. Ko, B. Kang, Y. Jung, J. Choi, H. Han, J. Gu, S. Cho, H. Kim, M. Bok, S. A. Park, J.-H. Jeong, I. Park, *Mater. Horiz.* **2023**, *10*, 4163.
[22] X. He, S. Yang, Q. Pei, Y. Song, C. Liu, T. Xu, X. Zhang, *ACS Sens.* **2020**, *5*, 1548.
[23] A. Khan, M. Winder, G. Hossain, *Biosens. Bioelectron.: X* **2022**, *10*, 100103.
[24] Y. Luo, Y. Li, P. Sharma, W. Shou, K. Wu, M. Foshey, B. Li, T. Palacios, A. Torralba, W. Matusik, *Nat. Electron.* **2021**, *4*, 193.
[25] M. D. Husain, S. Naqvi, O. Atalay, S. T. A. Hamdani, R. Kennon, *AATCC J. Res.* **2016**, *3*, 1.
[26] P. Lugoda, J. C. Costa, C. Oliveira, L. A. Garcia-Garcia, S. D. Wickramasinghe, A. Pouryazdan, D. Roggen, T. Dias, N. Münzenrieder, *Sensors* **2019**, *20*, 73.
[27] S. H. Jin, S.-K. Kang, I.-T. Cho, S. Y. Han, H. U. Chung, D. J. Lee, J. Shin, G. W. Baek, T.-i. Kim, J.-H. Lee, J. A. Rogers, *ACS Appl. Mater. Interfaces* **2015**, *7*, 8268.
[28] C. Xin, L. Chen, T. Li, Z. Zhang, T. Zhao, X. Li, J. Zhang, *IEEE Electron Device Lett.* **2018**, *39*, 1073.
[29] N. Kumar, J. Kumar, S. Panda, *AIP Adv.* **2015**, *5*, 6.
[30] S. B. Eadi, H. jin Shin, K. T. Nguyen, K.-W. Song, H.-W. Choi, S.-H. Kim, H.-D. Lee, *Sens. Actuators, B* **2022**, *353*, 131082.
[31] F. Catania, H. D. S. Oliveira, M. A. Costa Angeli, M. Ciocca, S. Pané, N. Münzenrieder, G. Cantarella, *Front. Electron.* **2022**, *2*, 786601.
[32] S. Choi, S. Kim, J. Jang, J. Kim, D. M. Kim, S.-J. Choi, H.-S. Mo, S. M. Lee, D. H. Kim, *IEEE Electron Device Lett.* **2019**, *40*, 1666.
[33] N. Munzenrieder, K. H. Cherenack, G. Troster, *IEEE Trans. Electron Devices* **2011**, *58*, 2041.
[34] G. Chen, X. Xiao, X. Zhao, T. Tat, M. Bick, J. Chen, *Chem. Rev.* **2021**, *122*, 3259.

[35] K. Schischke, N. F. Nissen, M. Schneider-Ramelow, *MRS Commun.* **2020**, *10*, 69.
[36] G. Genchi, M. S. Sinicropi, G. Lauria, A. Carocci, A. Catalano, *Int. J. Environ. Res. Public Health* **2020**, *17*, 3782.
[37] C. D. Hewitt, J. Savory, M. R. Wills, *Clin. Lab. Med.* **1990**, *10*, 403.
[38] L. M. Gaetke, C. K. Chow, *Toxicology* **2003**, *189*, 1.
[39] K. Mijnendonckx, N. Leys, J. Mahillon, S. Silver, R. Van Houdt, *Biometals* **2013**, *26*, 609.
[40] G. Hacisalihoglu, *Plants* **2020**, *9*, 1471.
[41] X.-N. Gu, Y.-F. Zheng, *Front. Mater. Sci. China* **2010**, *4*, 111.
[42] M. Dulal, S. Afroj, J. Ahn, Y. Cho, C. Carr, I.-D. Kim, N. Karim, *ACS Nano* **2022**, *16*, 19755.
[43] S. Ghosh, S. Mondal, S. Ganguly, S. Remanan, N. Singha, N. C. Das, *Fibers Polym.* **2018**, *19*, 1064.
[44] S. Ghosh, S. Ganguly, P. Das, T. K. Das, M. Bose, N. K. Singha, A. K. Das, N. C. Das, *Fibers Polym.* **2019**, *20*, 1161.
[45] A. Siddika, M. M. Hossain, J. Harmon, *ACS Sustainable Chem. Eng.* **2023**, *11*, 14913.
[46] A. H. Lanthaler, A. Carrasco-Pena, S. Krik, N. Münzenrieder, G. Cantarella, in *2024 IEEE International Conference on Flexible and Printable Sensors and Systems (FLEPS)*. IEEE, Piscataway, NJ **2024**, pp. 1–4.
[47] M. Li, Y. Wang, X. Fan, H. Huang, Y. Wan, Y. Li, J. Fang, J. Gao, Y. Yang, J. Liu, *ACS Appl. Mater. Interfaces* **2022**, *14*, 26958.
[48] S. Mura, G. Greppi, L. Malfatti, B. Lasio, V. Sanna, M. E. Mura, S. Marceddu, A. Lugliè, *J. Colloid Interface Sci.* **2015**, *456*, 85.
[49] J. R. Bautista-Quijano, P. Pötschke, H. Brünig, G. Heinrich, *Polymer* **2016**, *82*, 181.
[50] L. Bahin, M. Tourlonias, M.-A. Bueno, K. Sharma, R. M. Rossi, *Sens. Actuators, A* **2023**, *350*, 114117.
[51] S. K. Leist, D. Gao, R. Chiou, J. Zhou, *Virtual Phys. Prototyping* **2017**, *12*, 290.
[52] J. M. Toth, *Biocompatibility of PEEK polymers*, Elsevier, Amsterdam **2019**.
[53] P. Patel, T. R. Hull, R. E. Lyon, S. I. Stoliarov, R. N. Walters, S. Crowley, N. Safronava, *Polym. Degrad. Stab.* **2011**, *96*, 12.
[54] X. Tardif, B. Pignon, N. Boyard, J. W. Schmelzer, V. Sobotka, D. Delaunay, C. Schick, *Polym. Test.* **2014**, *36*, 10.
[55] M. Hasan, C. Cherif, A. Foisal, T. Onggar, R. Hund, A. Nocke, *Compos. Sci. Technol.* **2013**, *88*, 76.
[56] A. H. Lanthaler, F. Catania, H. D. S. Oliveira, C. Beltrami, A. Carrasco-Pena, M. Haller, N. Münzenrieder, G. Cantarella, in *2023 IEEE International Flexible Electronics Technology Conference (IFETC)*. IEEE, Piscataway, NJ **2023**, pp. 1–3.
[57] C.-M. Han, E.-J. Lee, H.-E. Kim, Y.-H. Koh, K. N. Kim, Y. Ha, S.-U. Kuh, *Biomaterials* **2010**, *31*, 3465.
[58] J. S. Heo, T. Kim, S.-G. Ban, D. Kim, J. H. Lee, J. S. Jur, M.-G. Kim, Y.-H. Kim, Y. Hong, S. K. Park, *Adv. Mater.* **2017**, *29*, 1701822.
[59] K. Chatterjee, J. Tabor, T. K. Ghosh, *Fibers* **2019**, *7*, 51.
[60] Y. Cheng, R. Wang, H. Zhai, J. Sun, *Nanoscale* **2017**, *9*, 3834.
[61] S. Takamatsu, T. Kobayashi, N. Shibayama, K. Miyake, T. Itoh, *Sens. Actuators, A* **2012**, *184*, 57.
[62] H. Galinski, D. Leutenegger, M. Amberg, F. Krogh, V. Schnabel, M. Heuberger, R. Spolenak, D. Hegemann, *Adv. Funct. Mater.* **2020**, *30*, 1910555.
[63] Z. Asfar, S. Nauman, G. ur Rehman, F. M. Malik, Y. Ayaz, N. Muhammad, *IEEE Sens. J.* **2016**, *16*, 8944.
[64] G. M. N. Islam, S. Collie, M. Qasim, M. A. Ali, *Nanomaterials* **2020**, *10*, 12.
[65] I. Verboven, J. Stryckers, V. Mecnika, G. Vandevenne, M. Jose, W. Deferme, *Materials* **2018**, *11*, 290.
[66] G. Paradossi, F. Cavalieri, E. Chiessi, C. Spagnoli, M. K. Cowman, *J. Mater. Sci.: Mater. Med.* **2003**, *14*, 687.
[67] C. DeMerlis, D. Schoneker, *Food Chem. Toxicol.* **2003**, *41*, 319.
[68] S. Jiang, J. Xu, Z. Chen, R. Guo, D. Miao, L. Peng, Y. Wang, S. Shang, *J. Mater. Sci.: Mater. Electron.* **2018**, *29*, 5624.
[69] J. Xu, S. Jiang, L. Peng, Y. Wang, S. Shang, D. Miao, R. Guo, *J. Ind. Text.* **2019**, *48*, 1545.
[70] S. Krishnaswamy, P. Panigrahi, P. P. Kala, S. Sofini, G. S. Nagarajan, *Heliyon* **2022**, *8*, 8.
[71] P. Zhao, Y. Song, P. Xie, F. Zhang, T. Xie, G. Liu, J. Zhao, S.-T. Han, Y. Zhou, *Adv. Funct. Mater.* **2023**, *33*, 2301816.
[72] M. Choi, Y. Kim, S. Park, D. Ka, T. Kim, S. Lee, E.-H. Sohn, Y. Jin, J. Hong, *Adv. Funct. Mater.* **2021**, *31*, 2101511.
[73] X. Zhang, L. Ke, X. Zhang, F. Xu, Y. Hu, H. Lin, J. Zhu, *ACS Appl. Mater. Interfaces* **2022**, *14*, 25753.
[74] Z. Liu, K. Chen, A. Fernando, Y. Gao, G. Li, L. Jin, H. Zhai, Y. Yi, L. Xu, Y. Zheng, H. Li, Y. Fan, Y. Li, Z. Zheng, *Chem. Eng. J.* **2021**, *403*, 126191.
[75] X. Guan, J. Gong, B. Xu, *ACS Appl. Mater. Interfaces* **2020**, *12*, 17967.
[76] Y. Wang, J. Wang, S. Cao, D. Kong, *J. Mater. Chem. C* **2019**, *7*, 9748.
[77] X. Liang, M. Zhu, H. Li, J. Dou, M. Jian, K. Xia, S. Li, Y. Zhang, *Adv. Funct. Mater.* **2022**, *32*, 2200162.
[78] X. Zhao, P. Zhang, S. Zhang, W. Yu, Z. Wang, N. Hu, L. Zhang, *Chem. Eng. J.* **2025**, *507*, 160736.
[79] E. A. McCullough, M. Kwon, H. Shim, *Meas. Sci. Technol.* **2003**, *14*, 1402.
[80] M. Li, K. Chang, W. Zhong, C. Xiang, W. Wang, Q. Liu, K. Liu, Y. Wang, Z. Lu, D. Wang, *Appl. Surf. Sci.* **2019**, *486*, 249.
[81] Z. Liu, K. Chen, A. Fernando, Y. Gao, G. Li, L. Jin, H. Zhai, Y. Yi, L. Xu, Y. Zheng, H. Li, Y. Fan, Y. Li, Z. Zheng, *Chem. Eng. J.* **2021**, *403*, 126191.
[82] Y. Chen, P. Schneider, A. Erbe, *Phys. Status Solidi A* **2012**, *209*, 846.
[83] M. Saif, S. Zhang, A. Haque, K. J. Hsia, *Acta Mater.* **2002**, *50*, 2779.
[84] C. Liu, C. Cai, J. Xie, W. Guo, H. Qin, P. Gao, H. Xiao, *Ceram. Int.* **2022**, *48*, 20627.
[85] B. Wen, J. E. Sader, J. J. Boland, *Phys. Rev. Lett.* **2008**, *101*, 175502.
[86] C.-C. Huang, Z.-K. Kao, Y.-C. Liao, *ACS Appl. Mater. Interfaces* **2013**, *5*, 12954.
[87] T. Nakajima, T. Tsuchiya, *J. Mater. Chem. C* **2015**, *3*, 3809.
[88] T. Nakajima, S. Hanawa, T. Tsuchiya, *J. Appl. Phys.* **2017**, *122*, 13.
[89] Q. Li, W. Zeng, Y. Li, *Sens. Actuators, B* **2022**, *359*, 131579.
[90] T. L. Guidotti, *Environ. Res.* **1978**, *15*, 443.
[91] J. H. Shorter, D. D. Nelson, J. B. McManus, M. S. Zahniser, S. R. Sama, D. K. Milton, *J. Breath Res.* **2011**, *5*, 037108.
[92] P. Barnes, S. Kharitonov, *Thorax* **1996**, *51*, 233.
[93] G. Cantarella, M. Madagalam, I. Merino, C. Ebner, M. Ciocca, A. Polo, P. Ibba, P. Bettotti, A. Mukhtar, B. Shkodra, S. A. Inam, A. J. Johnson, A. Pouryazdan, M. Paganini, R. Tiziani, T. Mimmo, S. Cesco, N. Münzenrieder, L. Petti, N. Cohen, P. Lugli, *Adv. Funct. Mater.* **2023**, *33*, 2210422.
[94] M. Irimia-Vladu, P. A. Troshin, M. Reisinger, L. Shmygleva, Y. Kanbur, G. Schwabegger, M. Bodea, R. Schwödiauer, A. Mumyatov, J. W. F. Fergus, V. F. Razumov, H. Sitter, N. S. Sarifici, S. Bauer, *Adv. Funct. Mater.* **2010**, *20*, 4069.
[95] A. Feteira, *J. Am. Ceram. Soc.* **2009**, *92*, 967.
[96] S. S. Phadkule, S. Sarma, *Polym. Compos.* **2023**, *44*, 1381.
[97] A. Nijkoops, D. Bhatt, A. Carrasco-Pena, Q. Z. Husain, N. Rapagnani, A. van Bezooijen, N. Cohen, G. Cantarella, N. Münzenrieder, *MRS Adv.* **2024**, *9*, 1560.
[98] N. S. Khaanghah, H. d. S. Oliveira, A. Carrasco-Pena, G. Cantarella, M. Haller, N. Rapagnani, A. van Bezooijen, M. Nippa, N. Münzenrieder, in *2023 IEEE SENSORS*, IEEE, Piscataway, NJ **2023**, pp. 01–04.
[99] Y. Lu, H. Zhang, Y. Zhao, H. Liu, Z. Nie, F. Xu, J. Zhu, W. Huang, *Adv. Mater.* **2024**, *36*, 2310613.
[100] R. Di Giacomo, C. Daraio, B. Maresca, *Proc. Natl. Acad. Sci. USA* **2015**, *112*, 4541.

[101] M. d. L. Nobre, S. Lanfredi, *Appl. Phys. Lett.* **2003**, *82*, 2284.
[102] J. Shin, B. Jeong, J. Kim, V. B. Nam, Y. Yoon, J. Jung, S. Hong, H. Lee, H. Eom, J. Yeo, J. Choi, D. Lee, S. H. Ko, *Adv. Mater.* **2020**, *32*, 1905527.
[103] F. T. Peirce, *J. Textile Instit. Trans.* **1930**, *21*, T377.
[104] S. Omeroglu, E. Karaca, B. Becerir, *Text. Res. J.* **2010**, *80*, 1180.
[105] N. Kenkare, T. May-Plumlee, *Int. J. Cloth. Sci. Technol.* **2005**, *17*, 109.
[106] A. R. Tehrani-Bagha, *Adv. Colloid Interface Sci.* **2019**, *268*, 114.
[107] Z. Suo, E. Ma, H. Gleskova, S. Wagner, *Appl. Phys. Lett.* **1999**, *74*, 1177.